Magneto-Stark effect of yellow excitons in cuprous oxide

Patric Rommel, Frank Schweiner,* and Jörg Main
Institut für Theoretische Physik 1, Universität Stuttgart, 70550 Stuttgart, Germany

Julian Heckötter, Marcel Freitag, Dietmar Fröhlich, Kevin Lehninger, Marc Aßmann, and Manfred Bayer
Experimentelle Physik 2, Technische Universität Dortmund, 44221 Dortmund, Germany

(Received 30 April 2018; revised manuscript received 17 July 2018; published 17 August 2018)

We investigate and compare experimental and numerical excitonic spectra of the yellow series in cuprous oxide (Cu_2O) in the Voigt configuration and thus partially extend the results of F. Schweiner *et al.* [Phys. Rev. B **95**, 035202 (2017)], who considered only the Faraday configuration. The main difference between the configurations is given by an additional effective electric field in the Voigt configuration, caused by the motion of the exciton through the magnetic field. This magneto-Stark effect was already postulated in 1961 by E. F. Gross *et al.* [Sov. Phys. Solid State 3, 221 (1961)] and D. G. Thomas and J. J. Hopfield [Phys. Rev. **124**, 657 (1961)]. Group-theoretical considerations show that, most of all, the field significantly increases the number of allowed lines by decreasing the symmetry of the system. This conclusion is supported by both the experimental and numerical data.

DOI: 10.1103/PhysRevB.98.085206

I. INTRODUCTION

Application of electric or magnetic fields, both representing well-controlled external perturbations, has offered detailed insight into quantum-mechanical systems by inducing characteristic shifts and lifting degeneracies of energy levels. This potential is apparent already for the simplest quantum-mechanical system in nature, the hydrogen atom, for which an external field reduces the symmetry from spherical to cylindrical [1–3].

In condensed matter, the hydrogen model is often applied as a simple, but nevertheless successful, model for problems in which the Coulomb interaction mediates the coupling between opposite charges of quasiparticles [4,5]. The most prominent example is the exciton, the bound complex of a negatively charged electron and a positively charged hole. In particular, for crystals of high symmetry such as cubic systems, the phenomenology of energy levels in an external field often resembles the corresponding hydrogen spectra after rescaling the energy axis with the corresponding material parameters that enter the Rydberg energy such as the effective mass and the dielectric constant, which in these systems are isotropic.

Recent high-resolution spectroscopy of excited exciton states in Cu_2O has allowed the revelation of features which result from the crystal environment with discrete instead of continuous symmetry, leading to deviations from a simple hydrogen description [6–8]. Theoretical investigations of excitons in external fields [9–11] also show differences from a simple hydrogen model. For example, the level degeneracy is lifted already at zero field. A detailed analysis shows that this splitting arises mostly from the complex valence band structure [12–15]. In effect, angular momentum is not a good quantum number anymore, but states of different angular momenta with the same parity are mixed. As the exciton size is large compared to that of the crystal unit cell, the mixing is weak, however, so that angular momentum may still be used approximately as a quantum number. Simply speaking, this can be understood in the following way: The exciton wave function averages over the crystal lattice, assembled by the cubic unit cells. With increasing wave function extension a state becomes less and less sensitive to the arrangement of the atoms in a crystal unit cell and thus to the deviations from spherical symmetry.

For example, the size of the cubic unit cell in Cu_2O is about 0.4 nm [16], while the Bohr radius is $a_{\mathrm{exc}} = 1.1\,\mathrm{nm}$ for the dipole-active P-type excitons dominating the absorption [17]. Using the formula $\langle r\rangle_{n,L} = \frac{1}{2}a_{\mathrm{exc}}[3n^2 - L(L+1)]$ [6], the size of the lowest exciton $n = 4$, for which the mixing becomes optically accessible, is $\langle r\rangle_{4,1} = 25.4\,\mathrm{nm}$, covering thousands of unit cells. As a consequence of the weak mixing, the state splitting is small compared to the separation between levels of different n. Generally, the average radius of the wave function increases as n^2, so that the zero-field state splitting decreases with increasing principal quantum number, leading to the levels becoming quasidegenerate again for n larger than about 10, as demonstrated in Ref. [7]. For smaller principal quantum numbers, the splitting can be well resolved, in particular, because the mixing of levels also causes a redistribution of oscillator strength, so that not only the P states but also higher-lying odd states such as $F, H, \ldots$ within a multiplet can be resolved in single-photon absorption.

Applying a magnetic field leads to a squeezing of the wave function mostly normal to the field, so that the influence of the crystal is enhanced. Even when assuming spatial isotropy, the symmetry is reduced to rotational invariance about the field, leaving only the magnetic quantum number m as a conserved quantity. As a consequence, states with the same m but different

*Present address: MINT-Kolleg, Universität Stuttgart, Stuttgart, Germany.

orbital angular momenta become mixed, activating further lines optically. In combination with the Zeeman splitting of the levels this leads to the rich appearance of the absorption spectra; in particular, like for excitons because their renormalized Rydberg energy is much smaller than in the atomic case, resonances between states of different principal quantum numbers can also be induced by the field application, at least for excited excitons.

As indicated above, a key ingredient for the renormalized Rydberg energy is the smaller masses of the involved particles forming an exciton, in particular of the hole compared to the nucleus. In Cu_2O, the electron mass is almost that of the free electron ($m_e = 0.99m_0$ [18]), while the hole represents the lighter particle ($m_h = 0.58m_0$ [18]), in contrast to most other semiconductors. This makes the reduced mass entering the relative motion of the electron and hole only a factor of less than 3 smaller than in hydrogen. The mass of the exciton center-of-mass motion, on the other hand, is clearly more than three orders of magnitude smaller. This raises the question of whether this mass disparity causes a difference in the optical spectra in the magnetic field, as the excitons are generated with a finite wave vector identical to the wave vector of the exciting laser.

In that respect two different field configurations need to be distinguished, namely, the Faraday and Voigt configurations. In the first case the magnetic field is applied along the optical axis, while in the second case the field is oriented normal to the optical axis. One would not expect a difference in the spectra between the two cases when probing atomic systems using a fixed polarization.

Here we have performed corresponding experiments which demonstrate that in contrast to the atomic case the exciton spectra differ significantly for the two field configurations. These findings are in good agreement with detailed theoretical calculations. From the comparison we trace the difference to the magneto-Stark effect [19–21], which acts only in the Voigt configuration, where the excited exciton is moving normal to the magnetic field, so that its two constituents are subject to the Lorentz force acting in opposite directions for an electron and a hole and therefore trying to move them apart, similar to the action of an electric field of the form

$$\mathcal{F}_{\mathrm{MSE}} = \frac{\hbar}{M}(\boldsymbol{K} \times \boldsymbol{B}), \tag{1}$$

where M is the exciton center of mass, $\boldsymbol{K}$ is the exciton wave vector, and $\boldsymbol{B}$ is the magnetic field. The action of this field is obviously absent in the Faraday configuration.

The main novelty in this work comes from the comparison of the spectra for atoms and for excitons. One would not expect any difference in the spectra for atoms when the magnetic field is aligned parallel or normal to the magnetic field. For excitons, on the other hand, it does make a difference, as we demonstrate here. Further, we identify the origin of this difference as the magneto-Stark Effect (MSE), which does not show up prominently for atoms due to their heavy mass and small size. The MSE was introduced theoretically in the 1960s [19–22], but clear demonstrations of its effect are still scarce [23].

The symmetry reduction by a longitudinal field (electric or magnetic) was also demonstrated in previous work. Still, in atomic physics, and also in semiconductor physics, it is a common belief that for a bulk crystal there should not be a difference between the two configurations as the symmetry reduction by the field is the same, considering only the impact of the magnetic field. The additional symmetry breaking here comes from the optical excitation, which in the Faraday configuration is parallel to the field, leading to no further symmetry reduction (as studied previously), while in the Voigt configuration the optical axis is normal to it. This lifts virtually all symmetries, as evidenced by the observation of basically all possible optical transitions, which therefore represents also a point of novelty.

In this respect we want to emphasize that the difference between the two field configurations that has been reported for confined semiconductor quantum structures has a different origin, as the geometric confinement breaks the spatial isotropy already at zero field. When applying a field, the energy spectrum of the free particles depends strongly on the field orientation [24]: For example, in a quantum well application of the field normal to the quantum well leads to a full discretization of the energy levels [15,25,26], while application in the well plane leaves the carrier motion along the field free (see Ref. [27] and references therein). Here one has a competition between the magnetic and geometric confinements normal to the field, while for normal orientation only the magnetic confinement is normal to the field. This causes an intrinsic difference of the magneto-optical spectra in terms of state energies. The same is true for other quantum structures like quantum dots, for which the geometric confinement in most cases is spatially anisotropic, while for the bulk the energy spectrum is independent of the field orientation [28]. We also note that in confined semiconductor quantum structures like quantum wells the difference in the spectra of the Faraday and Voigt configurations depends on the difference in the number of degrees of freedom involved in the interaction between the excitons and the magnetic field, i.e., two for the Faraday configuration and one for the Voigt configuration [29].

However, also for quantum structures one can indeed use the different field orientations to vary the number of observed optical transitions, somewhat similar to the case studied here. For example, in quantum wells or flat quantum dots the field orientation normal to the structure leaves the rotational in-plane symmetry about the field unchanged, while this symmetry is broken for application in the structural plane, so that one can mix excitons of different angular moments and make dark excitons visible [30].

II. HAMILTONIAN

Our theoretical description of excitonic spectra in Cu_2O with an external magnetic field builds upon Schweiner *et al.*'s treatment [13], in which only the Faraday configuration was considered. The Hamiltonian without magnetic field is given by

$$H = E_g + H_e(\boldsymbol{p}_e) + H_h(\boldsymbol{p}_h) + V(\boldsymbol{r}_e - \boldsymbol{r}_h), \tag{2}$$

where H_e and H_h are the kinetic energies of the electron and hole, respectively. They are given by

$$H_e(\boldsymbol{p}_e) = \frac{\boldsymbol{p}_e^2}{2m_e} \tag{3}$$

and

$$H_{\rm h}(\boldsymbol{p}_{\rm h}) = H_{\rm so} + (1/2\hbar^2 m_0)[\hbar^2(\gamma_1 + 4\gamma_2)\boldsymbol{p}_{\rm h}^2 + 2(\eta_1 + 2\eta_2)\boldsymbol{p}_{\rm h}^2(\boldsymbol{I}\cdot\boldsymbol{S}_{\rm h}) - 6\gamma_2\left(p_{\rm h1}^2\boldsymbol{I}_1^2 + \text{c.p.}\right) - 12\eta_2\left(p_{\rm h1}^2\boldsymbol{I}_1\boldsymbol{S}_{\rm h1} + \text{c.p.}\right) - 12\gamma_3(\{p_{\rm h1}, p_{\rm h2}\}\{\boldsymbol{I}_1, \boldsymbol{I}_2\} + \text{c.p.}) - 12\eta_3(\{p_{\rm h1}, p_{\rm h2}\}(\boldsymbol{I}_1\boldsymbol{S}_{\rm h2} + \boldsymbol{I}_2\boldsymbol{S}_{\rm h1}) + \text{c.p.})], \quad (4)$$

with the spin-orbit interaction

$$H_{\rm so} = \frac{2}{3}\Delta\left(1 + \frac{1}{\hbar^2}\boldsymbol{I}\cdot\boldsymbol{S}_{\rm h}\right). \quad (5)$$

Here, $\boldsymbol{I}$ is the quasispin, $\boldsymbol{S}_{\rm h}$ is the spin $S_{\rm h} = \frac{1}{2}$ of the hole, the anticommutator is given by $\{a, b\} = \frac{1}{2}(ab + ba)$, and c.p. denotes cyclic permutation. The electron and hole interact via the screened Coulomb potential

$$V(\boldsymbol{r}_{\rm e} - \boldsymbol{r}_{\rm h}) = -\frac{e^2}{4\pi\varepsilon_0\varepsilon|\boldsymbol{r}_{\rm e} - \boldsymbol{r}_{\rm h}|}, \quad (6)$$

with ε being the dielectric constant. To account for the magnetic field $\boldsymbol{B}$, we use the minimal substitutions $\boldsymbol{p}_{\rm e} \to \boldsymbol{p}_{\rm e} + e\boldsymbol{A}(\boldsymbol{r}_e)$ and $\boldsymbol{p}_{\rm h} \to \boldsymbol{p}_{\rm h} - e\boldsymbol{A}(\boldsymbol{r}_h)$ with the vector potential for a homogeneous field $\boldsymbol{A}(\boldsymbol{r}_{\rm e,h}) = (\boldsymbol{B}\times\boldsymbol{r}_{\rm e,h})/2$. The energy gained by the electron and hole spin in the external magnetic field is described by

$$H_B = \mu_{\rm B}[g_c\boldsymbol{S}_{\rm e} + (3\kappa + g_s/2)\boldsymbol{I} - g_s\boldsymbol{S}_{\rm h}]\cdot\boldsymbol{B}/\hbar, \quad (7)$$

with the Bohr magneton μ_B and the g factor of the hole spin $g_s \approx 2$. We finally switch to the center-of-mass reference frame [31]:

$$\begin{aligned}
\boldsymbol{r} &= \boldsymbol{r}_{\rm e} - \boldsymbol{r}_{\rm h},\\
\boldsymbol{R} &= \frac{m_{\rm e}}{m_{\rm e}+m_{\rm h}}\boldsymbol{r}_{\rm e} + \frac{m_{\rm h}}{m_{\rm e}+m_{\rm h}}\boldsymbol{r}_{\rm h},\\
\boldsymbol{p} &= \hbar\boldsymbol{k} - \frac{e}{2}\boldsymbol{B}\times\boldsymbol{R} = \frac{m_h}{m_{\rm e}+m_{\rm h}}\boldsymbol{p}_{\rm e} - \frac{m_{\rm e}}{m_{\rm e}+m_{\rm h}}\boldsymbol{p}_{\rm h},\\
\boldsymbol{P} &= \hbar\boldsymbol{K} + \frac{e}{2}\boldsymbol{B}\times\boldsymbol{r} = \boldsymbol{p}_{\rm e} + \boldsymbol{p}_{\rm h},
\end{aligned} \quad (8)$$

TABLE I. Material parameters used in Eqs. (2)–(8).

Parameter	Value	
Band gap energy	$E_{\rm g} = 2.17208\,\text{eV}$	[6]
Electron mass	$m_{\rm e} = 0.99\,m_0$	[18]
Hole mass	$m_{\rm h} = 0.58\,m_0$	[18]
Dielectric constant	$\varepsilon = 7.5$	[35]
Spin-orbit coupling	$\Delta = 0.131\,\text{eV}$	[12]
Valence band parameters	$\gamma_1 = 1.76$	[12]
	$\gamma_2 = 0.7532$	[12]
	$\gamma_3 = -0.3668$	[12]
	$\eta_1 = -0.020$	[12]
	$\eta_2 = -0.0037$	[12]
	$\eta_3 = -0.0337$	[12]
Fourth Luttinger parameter	$\kappa = -0.5$	[13]
g factor of the conduction band	$g_c = 2.1$	[36]

and we set $\boldsymbol{R} = 0$. More details can be found in Refs. [13,32–34], and the values of the material parameters for Cu_2O used in Eqs. (2)–(8) are listed in Table I.

Faraday and Voigt configurations: Magneto-Stark effect

We consider two different relative orientations of the magnetic field to the optical axis. In the Faraday configuration, both axes are aligned to be parallel, whereas in the Voigt configuration, they are orthogonal to each other. Generally, the exciting laser will transfer a finite momentum $\hbar\boldsymbol{K}$ onto the exciton. This center-of-mass momentum would have to be added in the terms for the kinetic energies. Even without a magnetic field, this leads to quite complicated formulas (see the expressions for the Hamiltonian in the Supplemental Material of Ref. [37]) which are further complicated by the minimal substitution. Since the effect of many of the arising terms is presumably negligible due to the smallness of K, we simplify the problem and consider only the leading term [3,38],

$$H_{\rm ms} = \frac{\hbar e}{M}(\boldsymbol{K}\times\boldsymbol{B})\cdot\boldsymbol{r}, \quad (9)$$

in our numerical calculations, which is the well-known motional Stark effect term of the hydrogen atom. This term has the same effect as an external electric field (1) perpendicular to the plane spanned by the wave vector $\boldsymbol{K}$ and the magnetic field vector $\boldsymbol{B}$. Evidently then, the significance of this term depends on the configuration.

For the Faraday configuration, the effective electrical field (1) vanishes. A previous investigation by Schweiner *et al.* [13] was thus conducted under the approximation of vanishing center-of-mass momentum. They report a complicated splitting pattern where the magnetic field lifts all degeneracies. For a magnetic field oriented along one of the high-symmetry axes of the crystal, the symmetry of the exciton is reduced from $O_{\rm h}$ to $C_{4\rm h}$. Still, some selection rules remain and not all lines become dipole allowed. Parity remains a good quantum number, and since only states with an admixture of P states have nonvanishing oscillator strengths, only states with odd values of L contribute to the exciton spectrum.

In the Voigt configuration, on the other hand, the excitons have a nonvanishing momentum perpendicular to the magnetic field, and the magneto-Stark term has to be included. For our calculations, we therefore include an electric field, the size of which is given by the wave vector $K_0 = 2.79\times10^7\,\frac{1}{\rm m}$ of the incident light and the magnetic field. This value is obtained with the condition

$$\frac{\hbar c K_0}{\sqrt{\varepsilon_{b2}}} = E_g - \frac{R_{\rm exc}}{n^2} \quad (10)$$

for $n = 5$ and with $\varepsilon_{b2} = 6.46$ [35] and $R_{\rm exc} = 86\,\text{meV}$ [12]; that is, $\hbar K_0$ is the momentum of a photon that has the appropriate energy to create an exciton in the energy range we consider. Note that, in contrast to Table I, we here use the dielectric constant in the high-frequency limit to describe the refractive index of the incident light. Since the total mass M of the exciton is some three orders of magnitudes smaller than that of a hydrogen atom, this term will have a significant effect on the spectra, even more so if we consider that the region of high fields is shifted to much lower values for the exciton

[13]. The term (9) breaks the inversion symmetry, and parity ceases to be a good quantum number. While in the Faraday configuration only the dipole-allowed exciton states with odd angular momentum were important, now the states with even angular momentum also need to be considered. Hence, we need to include the terms for the central-cell corrections with the Haken potential as given in Refs. [33,37] in our treatment to correctly take the coupling to the low-lying S states into account.

In general, polariton effects have to be considered when the center-of-mass momentum $\boldsymbol{K}$ is nonzero. The experimental results in Refs. [39–41], on the other hand, show that the polariton effects for the $1S$ state are of the order of 10 μeV and thus small in comparison with the effects considered in this paper. Furthermore, a recent discussion by Stolz *et al.* [42] concluded that polariton effects should be observable in transmission experiments only for $n \geqslant 28$. Hence, we will not include them in our discussion.

III. NUMERICAL APPROACH

Using the Hamiltonian (2) with the additional terms for the central-cell corrections H_{CCC} and the magneto-Stark effect H_{ms} with a suitable set of basis vectors, the Schrödinger equation can be brought into the form of a generalized eigenvalue equation

$$\boldsymbol{D}\boldsymbol{c} = E\boldsymbol{M}\boldsymbol{c}. \tag{11}$$

We choose a basis consisting of Coulomb-Sturmian functions with an appropriate part for the various appearing spins and angular momenta. Due to the broken inversion symmetry, it is not sufficient to include only basis functions of odd parity as in Ref. [13]. Instead, basis functions of even symmetry have to be included as well. The resulting equation can then be solved using a suitable LAPACK routine [43]. For details we refer to the discussions in Refs. [13,33,44].

Oscillator strengths

The extraction of the dipole oscillator strengths is performed analogously to the calculation for the Faraday configuration [13]. For the relative oscillator strengths we use

$$f_{\mathrm{rel}} \sim \left| \lim_{r\to 0} \frac{\partial}{\partial r} \langle \pi_{x,z} | \Psi(\boldsymbol{r}) \rangle \right|^2 \tag{12}$$

for light linearly polarized in the x or z direction. The states $|\pi_{x,z}\rangle$ are given by

$$|\pi_x\rangle = \frac{i}{\sqrt{2}}[|2,\ -1\rangle_D + |2,\ 1\rangle_D], \tag{13a}$$

$$|\pi_z\rangle = \frac{i}{\sqrt{2}}[|2,\ -2\rangle_D - |2,\ 2\rangle_D], \tag{13b}$$

where $|F_t,\ M_{F_t}\rangle_D$ is an abbreviation [13] for

$$\begin{aligned} &|(S_{\mathrm{e}},\ S_{\mathrm{h}})\,S,\ I;\ I+S,\ L;\ F_t,\ M_{F_t}\rangle \\ &\quad = |(1/2,\ 1/2)\,0,\ 1;\ 1,\ 1;\ F_t,\ M_{F_t}\rangle. \end{aligned} \tag{14}$$

In this state, the electron and hole spins S_{e} and S_{h} are coupled to the total spin S. This is combined first with the quasispin I and then with the orbital angular momentum L to obtain the total angular momentum F_t. M_{F_t} is the projection onto the axis of quantization.

IV. EXPERIMENT

In the experiment, we investigated the absorption of thin Cu_2O crystal slabs. Three different samples with different orientations were available: In the first sample the [001] direction is normal to the crystal surface; in the other two samples the normal direction corresponds to the [110] and [111] orientations. The thicknesses of these samples differed slightly from 30 to 50 μm, which is, however, of no relevance for the results described below. For application of a magnetic field, the samples were inserted at a temperature of 1.4 K in an optical cryostat with a superconducting split-coil magnet. Magnetic fields with strengths up to 7 T could be applied with orientation either parallel to the optical axis (Faraday configuration) or normal to the optical axis (Voigt configuration).

The absorption was measured using a white-light source which was filtered by a double monochromator such that only the range of energies in which the exciton states of interest are located was covered. A linear polarization of the exciting light, hitting the crystal normal to the slabs, was used. The transmitted light was dispersed by another double monochromator and detected by a liquid-nitrogen-cooled charge-coupled-device camera, providing a spectral resolution of about 10 μeV. Since the spectral width of the studied exciton resonances is significantly larger than this value, the setup provides sufficient resolution.

V. RESULTS AND DISCUSSION

Figure 1 shows experimental spectra for $n = 4$ to $n = 7$ in the Voigt configuration with polarization orthogonal and parallel to the magnetic field. The spectra for the two cases show clear differences due to the different selection rules for different polarizations. We will show below that all lines, in principle, become dipole allowed and can be excited by exactly one of the two polarizations shown here.

For the comparison between the Faraday and Voigt configurations we show in Fig. 2 experimental spectra taken in the Voigt configuration [Fig. 2(a)] and in the Faraday configuration [Fig. 2(b)] with polarization orthogonal to the magnetic field. The polarizations are chosen in such a way that the same selection rules would apply to both spectra in Fig. 2 without the magneto-Stark field. Thus, the differences between them must be due to the different geometries. S lines are visible for both configurations. This can be attributed to quadrupole-allowed transitions in the case of the Faraday configuration [13]. For the Voigt configuration, these lines quickly fade away. This is a sign that the additional mixing from the electric field transfers quadrupole oscillator strength away from the S excitons. This effect is not reproduced in the numerical spectra since we extracted only dipole oscillator strengths. In general, the effective electric field lifts selection rules, revealing additional lines not visible in the Faraday configuration. This can, for example, clearly be seen for the $n = 5$ states.

In Figs. 3 and 4 we show a comparison between experimental and numerically obtained line positions for $n = 4$ and $n = 5$. To improve the presentation of areas with many densely

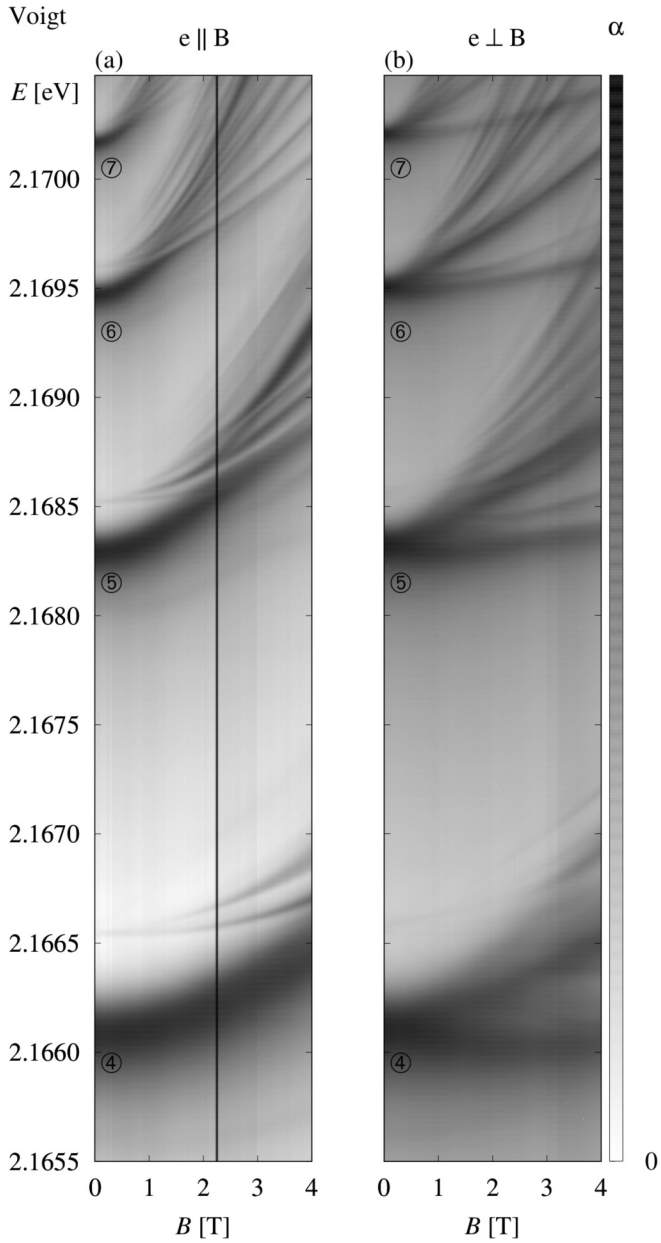

FIG. 1. Experimental transmission spectra in arbitrary units for $n = 4$ to $n = 7$ taken in the Voigt configuration for polarization (a) orthogonal [010] and (b) parallel [100] to the magnetic field.

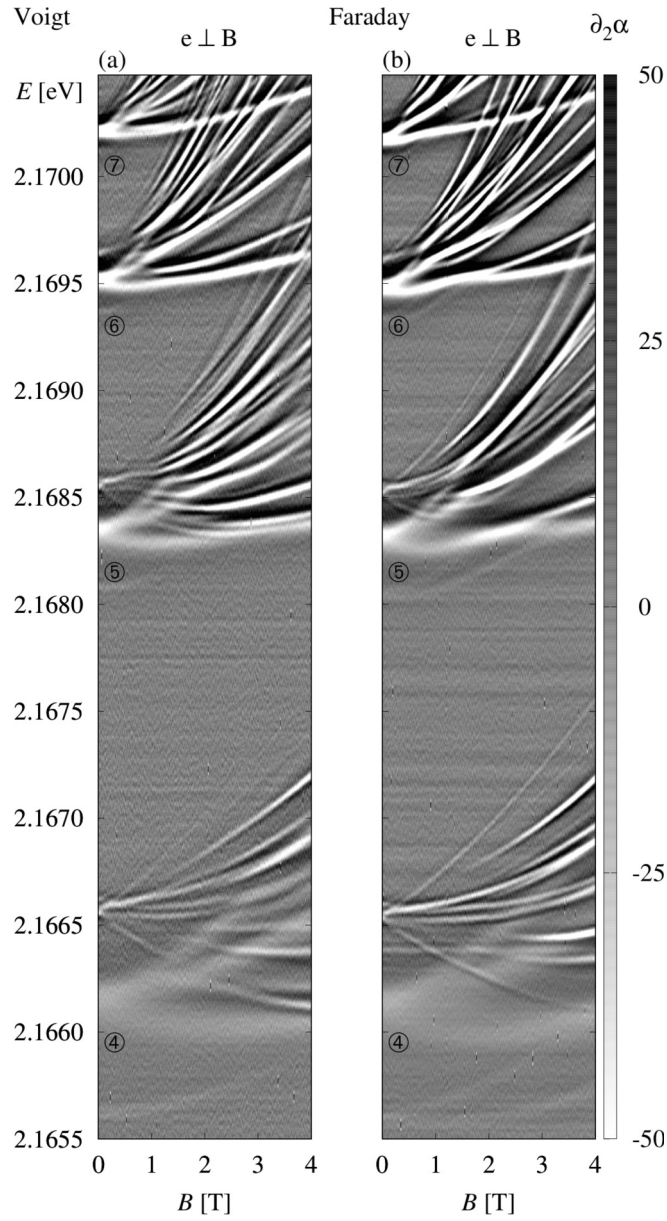

FIG. 2. Second derivative of experimental transmission spectra for $n = 4$ to $n = 7$ taken in the (a) Voigt configuration and (b) Faraday configuration with polarization orthogonal [010] to the magnetic field. Data for the Faraday configuration were obtained by combining σ^+- and σ^--polarized spectra from Ref. [13] in an appropriate linear combination. We use the second derivative for better visibility of weak lines.

lying lines that individually have very low oscillator strengths, numerical spectra are convoluted using a Gaussian function with a constant width of 13.6 μeV. This value is of the same order of magnitude as the width of the sharpest lines visible in the experiment. While the position of the P and F lines is reproduced very well, noticeable disagreement is observed for the S lines and also the faint $4D$ line visible in Fig. 4. Since our model is not explicitly constructed on a lattice [45], we have to include the central-cell corrections as an approximation in our Hamiltonian. As the central-cell corrections influence the even-parity states much more strongly than the odd-parity states, the error involved in this is more pronounced for the former than for the latter. A similar effect can also be seen in Ref. [33]. To make additional comparisons involving the oscillator strengths possible we also present in Fig. 5(a) data with light linearly polarized orthogonally [010] to the magnetic field in the Faraday configuration taken from Ref. [13] and in Figs. 5(b) and 5(c) spectra in the Voigt configuration with light polarized orthogonally [010] and parallel [100] to the magnetic field axis, respectively, for the principal quantum numbers $n = 4$ and $n = 5$. The experimental absorption coefficients do not fall to zero far away from the peaks due to the phonon background. We lowered the values with a constant shift to counteract this effect. Note that we investigate a parameter

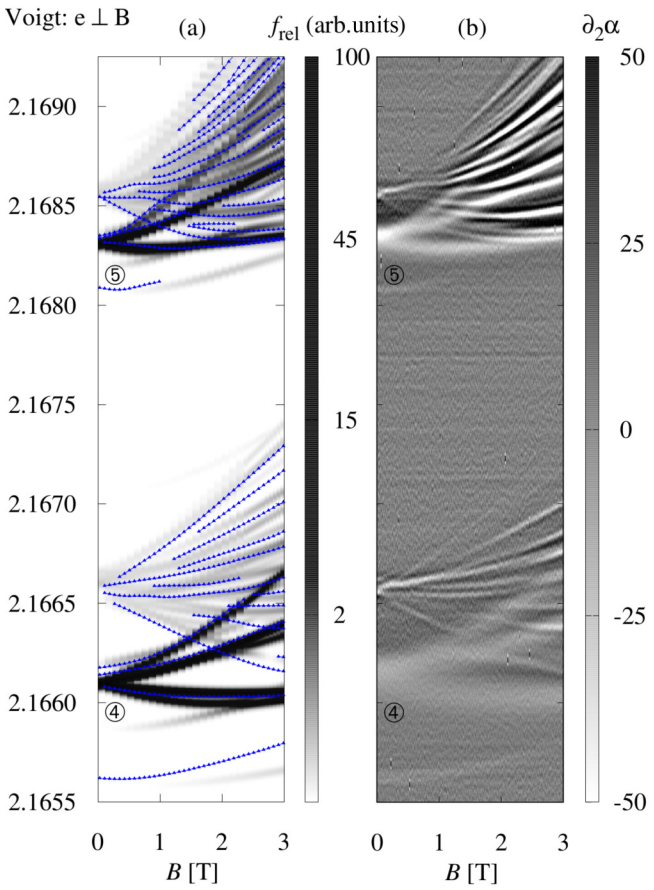

FIG. 3. Comparison between numerical and experimental line positions for the Voigt configuration with light polarized orthogonally [010] to the magnetic field. (a) Numerical data in gray scale with read-out experimental line positions (blue triangles) and (b) experimental data using the second derivative to enhance visibility of weak lines. Note that the resolution of the numerical data is not uniform for all field strengths.

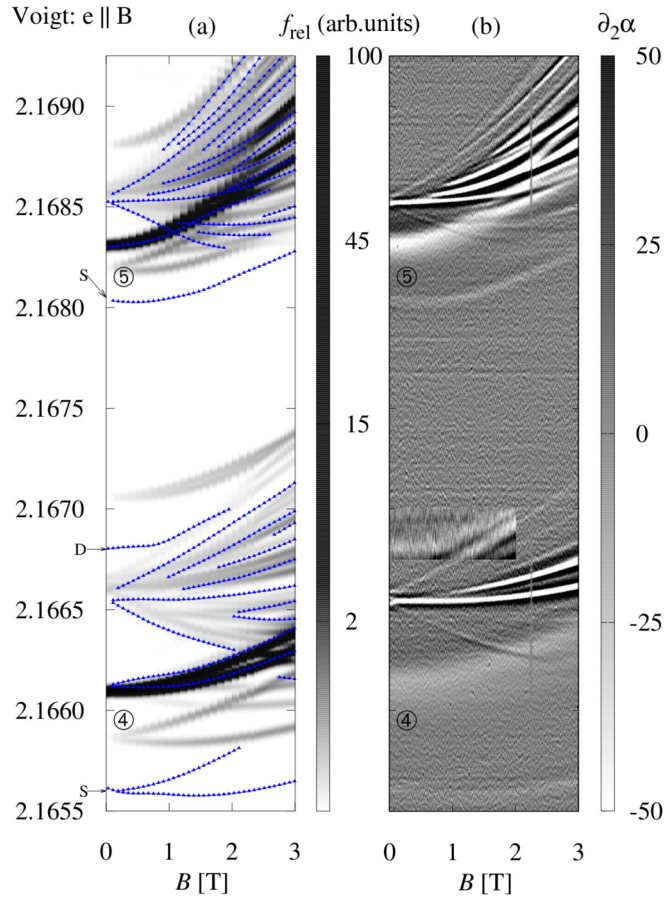

FIG. 4. Comparison between numerical and experimental line positions for the Voigt configuration with light polarized parallel [100] to the magnetic field. (a) Numerical data in greyscale with read out experimental line positions (blue triangles) and (b) experimental data using the second derivative to enhance visibility of weak lines. We increase the visibility of the experimental 4D line by using a different filter width and higher contrast. Note that the resolution of the numerical data is not uniform for all field strengths.

region where the effects of quantum chaos as discussed in Ref. [46] are not important.

In general, good agreement between the experimental and numerical data sets is obtained. In the Voigt configuration in Figs. 3, 4, and 5, a rich splitting is observed, especially of the F states of the $n = 5$ excitons. We see that light polarized orthogonally to the magnetic field probes lines complementary to the ones excited by light polarized in the direction of the field, a result that will also follow from our discussion below.

In experiment, we are not able to resolve the multiplicity of lines that the calculations reveal. This is related to the increased linewidth of the individual features arising from exciton relaxation by radiative decay and phonon scattering, which are not included in the model. Still, the field dependences of the main peaks with the largest oscillator strength are nicely reproduced, as are the broadenings of the multiplets due to level splitting.

Influence of the magneto-Stark effect

In this section we discuss the effects of the additional effective electric field on the line spectra. As we will see in the following group-theoretical derivations, the most pronounced effect is a significant increase in the number of dipole-allowed lines due to the decreased symmetry with the electric field. Figures 5(a) and 5(b) show this quite clearly, especially for the large number of additional F lines and also G lines for $n = 5$ in the Voigt configuration. This is most obvious for the theoretical spectra but can also distinctly be seen in the experiment for $n = 5$. Note that without the magneto-Stark effect the same selection rules would apply to the spectra in Figs. 5(a) and 5(b) but not in Fig. 5(c). In contrast to the Faraday configuration [13], we cannot limit ourselves to the states with odd values for L, owing to the mixture of the even and odd series in the electric field. We discuss the case of a magnetic field aligned in the [001] direction and will disregard the influence of the central-cell corrections in this discussion.

We consider the reduction of the irreducible representations $\tilde{D}^{F\pm}$ of the full rotation group in the presence of the crystal as well as the magnetic and effective electric fields, where $F = J + L = (I + S_h) + L$ is the angular momentum without the electron spin. Here, the quasispin I and hole spin S_h are first coupled to the effective hole spin J and then combined

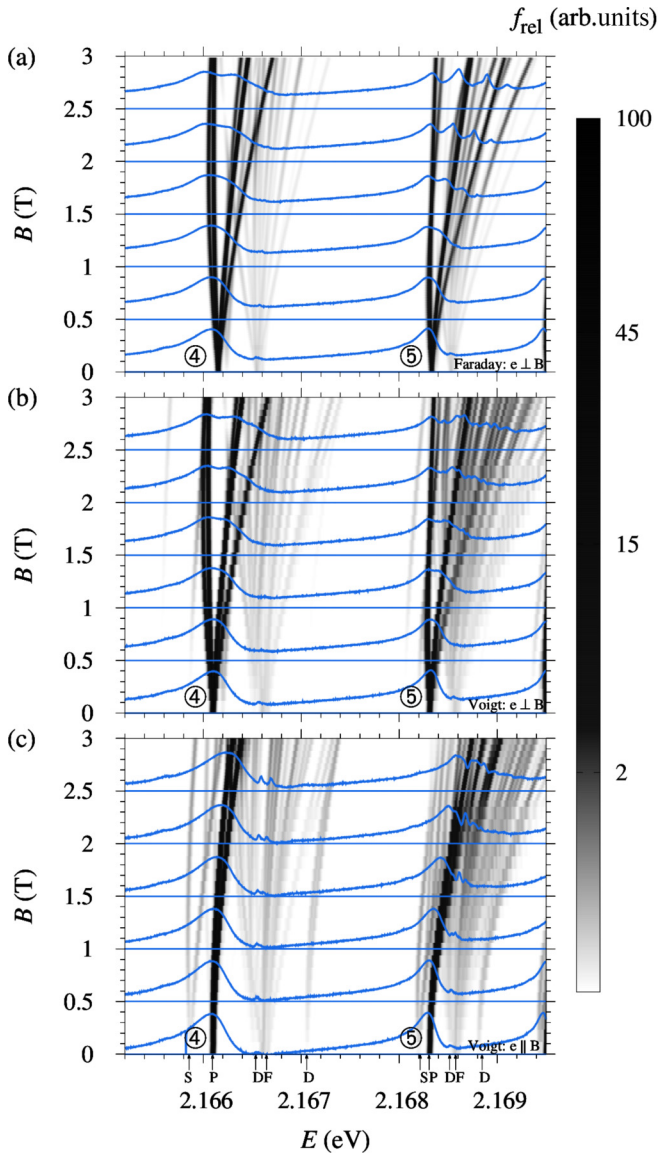

FIG. 5. Comparison of numerical and experimental spectra of the $n = 4$ and $n = 5$ excitons in an external magnetic field $\mathbf{B} \parallel [100]$. (a) Faraday configuration with light polarized along the [010] direction. Data were obtained by combining σ^+- and σ^--polarized spectra from Ref. [13] in an appropriate linear combination. Voigt configuration with a wave vector aligned with the [001] direction and the light polarized (b) orthogonally [010] and (c) parallel [100] to the magnetic field. Numerically calculated relative oscillator strengths are shown in gray scale in arbitrary units. Experimentally measured absorption coefficients α are superimposed in arbitrary units for a few selected values of B (blue solid lines). Note that the resolution of the numerical data is not uniform for all field strengths. We point out the theoretical visibility of S and D excitons as marked in (c). See text for further information.

with the orbital angular momentum L to form F. With this information we will be able to deduce the splitting of the lines due to the reduced symmetry [47]. Additionally, we can compare the resulting irreducible representations with those that the dipole operator belongs to. This will tell us which lines are dipole allowed and which are not. Note that the symmetry of the quasispin I in O_h is given by $\Gamma_5^+ = \Gamma_4^+ \otimes \Gamma_2^+$ [13], and therefore, all irreducible representations have to be multiplied by Γ_2^+ in comparison with the case of an ordinary spin. Keeping this in mind, we have [48]

$$L = 0:$$
$$\tilde{D}^{\frac{1}{2}+} = D^{\frac{1}{2}+} \otimes \Gamma_2^+ = \Gamma_6^+ \otimes \Gamma_2^+ = \Gamma_7^+, \tag{15a}$$
$$L = 1:$$
$$\tilde{D}^{\frac{1}{2}-} = D^{\frac{1}{2}-} \otimes \Gamma_2^+ = \Gamma_6^- \otimes \Gamma_2^+ = \Gamma_7^-, \tag{15b}$$
$$\tilde{D}^{\frac{3}{2}-} = D^{\frac{3}{2}-} \otimes \Gamma_2^+ = \Gamma_8^- \otimes \Gamma_2^+ = \Gamma_8^-, \tag{15c}$$
$$L = 2:$$
$$\tilde{D}^{\frac{3}{2}+} = D^{\frac{3}{2}+} \otimes \Gamma_2^+ = \Gamma_8^+ \otimes \Gamma_2^+ = \Gamma_8^+, \tag{15d}$$
$$\tilde{D}^{\frac{5}{2}+} = D^{\frac{5}{2}+} \otimes \Gamma_2^+ = (\Gamma_7^+ \oplus \Gamma_8^+) \otimes \Gamma_2^+ = \Gamma_6^+ \oplus \Gamma_8^+, \tag{15e}$$
$$L = 3:$$
$$\tilde{D}^{\frac{5}{2}-} = D^{\frac{5}{2}-} \otimes \Gamma_2^+ = (\Gamma_7^- \oplus \Gamma_8^-) \otimes \Gamma_2^+ = \Gamma_6^- \oplus \Gamma_8^-, \tag{15f}$$
$$\tilde{D}^{\frac{7}{2}-} = D^{\frac{7}{2}-} \otimes \Gamma_2^+ = (\Gamma_6^- \oplus \Gamma_7^- \oplus \Gamma_8^-) \otimes \Gamma_2^+ = \Gamma_7^- \oplus \Gamma_6^- \oplus \Gamma_8^-, \tag{15g}$$
$$L = 4:$$
$$\tilde{D}^{\frac{7}{2}+} = D^{\frac{7}{2}+} \otimes \Gamma_2^+ = (\Gamma_6^+ \oplus \Gamma_7^+ \oplus \Gamma_8^+) \otimes \Gamma_2^+ = \Gamma_7^+ \oplus \Gamma_6^+ \oplus \Gamma_8^+, \tag{15h}$$
$$\tilde{D}^{\frac{9}{2}+} = D^{\frac{9}{2}+} \otimes \Gamma_2^+ = (\Gamma_6^+ \oplus \Gamma_8^+ \oplus \Gamma_8^+) \otimes \Gamma_2^+ = \Gamma_7^+ \oplus \Gamma_8^+ \oplus \Gamma_8^+. \tag{15i}$$

We still need to include the spin of the electron which transforms according to Γ_6^+. For vanishing magnetic field strengths, the representations belonging to an irreducible representation without the spin are degenerate. Those will be written in brackets. The reduction [48] will be specified only for even parity since the odd case changes only the sign. We obtain

$$\tilde{D}^{\frac{1}{2}+} \otimes \Gamma_6^+ = (\Gamma_2^+ \oplus \Gamma_5^+), \tag{16a}$$
$$\tilde{D}^{\frac{3}{2}+} \otimes \Gamma_6^+ = (\Gamma_3^+ \oplus \Gamma_4^+ \oplus \Gamma_5^+), \tag{16b}$$
$$\tilde{D}^{\frac{5}{2}+} \otimes \Gamma_6^+ = (\Gamma_1^+ \oplus \Gamma_4^+) \oplus (\Gamma_3^+ \oplus \Gamma_4^+ \oplus \Gamma_5^+), \tag{16c}$$
$$\tilde{D}^{\frac{7}{2}+} \otimes \Gamma_6^+ = (\Gamma_2^+ \oplus \Gamma_5^+) \oplus (\Gamma_1^+ \oplus \Gamma_4^+) \oplus (\Gamma_3^+ \oplus \Gamma_4^+ \oplus \Gamma_5^+), \tag{16d}$$
$$\tilde{D}^{\frac{9}{2}+} \otimes \Gamma_6^+ = (\Gamma_2^+ \oplus \Gamma_5^+) \oplus (\Gamma_3^+ \oplus \Gamma_4^+ \oplus \Gamma_5^+) \oplus (\Gamma_3^+ \oplus \Gamma_4^+ \oplus \Gamma_5^+). \tag{16e}$$

Γ_1^+ and Γ_2^+ are one-dimensional, Γ_3^+ is two-dimensional, and Γ_4^+ and Γ_5^+ are three-dimensional. So without the field we have, for example, fourfold degenerate S states and P states that are split into one fourfold and one eightfold degenerate line. If the magnetic field is switched on, the electric field becomes

nonvanishing too. The symmetry is reduced from O_h to C_S [48]. All representations of C_S are one-dimensional, so all degeneracies will be lifted, just as in the case with only a magnetic field. But in contrast to the Faraday configuration, the symmetry is lowered even further, leading to a greater mixture of the states. In fact, all lines become dipole allowed. To see this, we have to consider the reduction of the irreducible representations of O_h in C_S [47,48]. The relevant expressions are

$$\begin{aligned}
\Gamma_1^+ &\to \Gamma_1, & \Gamma_1^- &\to \Gamma_2,\\
\Gamma_2^+ &\to \Gamma_1, & \Gamma_2^- &\to \Gamma_2,\\
\Gamma_3^+ &\to \Gamma_1 \oplus \Gamma_1, & \Gamma_3^- &\to \Gamma_2 \oplus \Gamma_2,\\
\Gamma_4^+ &\to \Gamma_1 \oplus \Gamma_2 \oplus \Gamma_2, & \Gamma_4^- &\to \Gamma_2 \oplus \Gamma_1 \oplus \Gamma_1,\\
\Gamma_5^+ &\to \Gamma_1 \oplus \Gamma_2 \oplus \Gamma_2, & \Gamma_5^- &\to \Gamma_2 \oplus \Gamma_1 \oplus \Gamma_1.
\end{aligned}$$

The dipole operator belongs to Γ_4^- in O_h [48], and its reduction therefore includes all appearing representations. Thus, all $4n^2$ lines receive nonvanishing oscillator strength, with the only limitation being given by the polarization of the incident light; that is, a given state can be excited either by radiation polarized in the z direction (Γ_2) or by radiation polarized in the x-y plane (Γ_1).

VI. SUMMARY

We extended the previous work by Schweiner *et al.* [13] on the optical spectra of magnetoexcitons in cuprous oxide to the Voigt configuration and showed that the nonvanishing exciton momentum perpendicular to the magnetic field leads to the appearance of an effective magneto-Stark field. Including the valance band structure and taking into account central-cell corrections as well as the Haken potential allowed us to produce numerical results in good agreement with experimental absorption spectra. We observe a significant increase in the number of visible lines in both our experimental and our numerical data compared to the Faraday configuration. Using group-theoretical methods, we show that this is related to the magneto-Stark field increasing the mixing between states. While their positions remain relatively unaffected, the mixing of states leads to finite oscillator strength of, at least in principle, all lines.

ACKNOWLEDGMENTS

This work was supported by Deutsche Forschungsgemeinschaft (Grants No. MA1639/13-1 and No. AS459/3-1).

[1] H. Friedrich and D. Wintgen, Phys. Rep. **183**, 37 (1989).
[2] H. Hasegawa, M. Robnik, and G. Wunner, Prog. Theor. Phys. Suppl. **98**, 198 (1989).
[3] H. Ruder, G. Wunner, H. Herold, and F. Geyer, *Atoms in Strong Magnetic Fields: Quantum Mechanical Treatment and Applications in Astrophysics and Quantum Chaos*, Astronomy and Astrophysics Library (Springer, Berlin, 1994).
[4] G. H. Wannier, Phys. Rev. **52**, 191 (1937).
[5] R. Knox, *Theory of Excitons*, Solid State Physics Supplement Vol. 5 (Academic, New York, 1963).
[6] T. Kazimierczuk, D. Fröhlich, S. Scheel, H. Stolz, and M. Bayer, Nature (London) **514**, 343 (2014).
[7] J. Thewes, J. Heckötter, T. Kazimierczuk, M. Aßmann, D. Fröhlich, M. Bayer, M. A. Semina, and M. M. Glazov, Phys. Rev. Lett. **115**, 027402 (2015).
[8] J. Heckötter, M. Freitag, D. Fröhlich, M. Aßmann, M. Bayer, M. A. Semina, and M. M. Glazov, Phys. Rev. B **95**, 035210 (2017).
[9] S. Zielińska-Raczyńska, D. Ziemkiewicz, and G. Czajkowski, Phys. Rev. B **94**, 045205 (2016).
[10] S. Zielińska-Raczyńska, D. Ziemkiewicz, and G. Czajkowski, Phys. Rev. B **95**, 075204 (2017).
[11] M. Kurz, P. Grünwald, and S. Scheel, Phys. Rev. B **95**, 245205 (2017).
[12] F. Schöne, S.-O. Krüger, P. Grünwald, H. Stolz, S. Scheel, M. Aßmann, J. Heckötter, J. Thewes, D. Fröhlich, and M. Bayer, Phys. Rev. B **93**, 075203 (2016).
[13] F. Schweiner, J. Main, G. Wunner, M. Freitag, J. Heckötter, C. Uihlein, M. Aßmann, D. Fröhlich, and M. Bayer, Phys. Rev. B **95**, 035202 (2017).
[14] F. Schweiner, J. Main, M. Feldmaier, G. Wunner, and C. Uihlein, Phys. Rev. B **93**, 195203 (2016).
[15] G. E. W. Bauer and T. Ando, Phys. Rev. B **38**, 6015 (1988).
[16] P. Korzhavyi, *Literature Review on the Properties of Cuprous Oxide Cu2O and the Process of Copper Oxidation*, SKB Technical Report (Svensk Kärnbränslehantering AB, Solna, Sweden, 2011).
[17] G. M. Kavoulakis, Y.-C. Chang, and G. Baym, Phys. Rev. B **55**, 7593 (1997).
[18] J. W. Hodby, T. E. Jenkins, C. Schwab, H. Tamura, and D. Trivich, J. Phys. C **9**, 1429 (1976).
[19] E. F. Gross, B. P. Zakharchenko, and O. V. Konstantinov, Sov. Phys. Solid State **3**, 221 (1961).
[20] J. J. Hopfield and D. G. Thomas, Phys. Rev. **122**, 35 (1961).
[21] D. G. Thomas and J. J. Hopfield, Phys. Rev. **124**, 657 (1961).
[22] A. G. Zhilich, J. Halpern, and B. P. Zakharchenya, Phys. Rev. **188**, 1294 (1969).
[23] M. Lafrentz, D. Brunne, A. V. Rodina, V. V. Pavlov, R. V. Pisarev, D. R. Yakovlev, A. Bakin, and M. Bayer, Phys. Rev. B **88**, 235207 (2013).
[24] V. M. Agranovich, A. A. Maradudin, G. Landwehr, and E. I. Rashba, *Landau Level Spectroscopy*, Modern Problems in Condensed Matter Sciences Vols. 27.1 and 27.2 (North-Holland, Amsterdam, 1991).
[25] J. C. Maan, G. Belle, A. Fasolino, M. Altarelli, and K. Ploog, Phys. Rev. B **30**, 2253 (1984).
[26] G. E. W. Bauer and T. Ando, Phys. Rev. B **37**, 3130 (1988).
[27] M. Bayer, A. A. Dremin, V. D. Kulakovskii, A. Forchel, F. Faller, P. A. Knipp, and T. L. Reinecke, Phys. Rev. B **52**, 14728 (1995).
[28] P. D. Wang, J. L. Merz, S. Fafard, R. Leon, D. Leonard, G. Medeiros-Ribeiro, M. Oestreich, P. M. Petroff, K. Uchida, N. Miura, H. Akiyama, and H. Sakaki, Phys. Rev. B **53**, 16458 (1996).
[29] G. Czajkowski, F. Bassani, and L. Silvestri, Riv. Nuovo Cimento **26**, 1 (2003).

[30] M. Bayer, O. Stern, A. Kuther, and A. Forchel, Phys. Rev. B **61**, 7273 (2000).
[31] P. Schmelcher and L. S. Cederbaum, Z. Phys. D: At., Mol. Clusters **24**, 311 (1992).
[32] F. Schweiner, J. Main, and G. Wunner, Phys. Rev. B **93**, 085203 (2016).
[33] F. Schweiner, J. Main, G. Wunner, and C. Uihlein, Phys. Rev. B **95**, 195201 (2017).
[34] J. M. Luttinger, Phys. Rev. **102**, 1030 (1956).
[35] *Landolt-Börnstein - Group III Condensed Matter*, edited by O. Madelung, U. Rössler, and M. Schulz (Springer, Berlin, 1998).
[36] S. L. Artyukhin, Ph.D. thesis, Rijksuniversiteit Groningen, 2012.
[37] F. Schweiner, J. Ertl, J. Main, G. Wunner, and C. Uihlein, Phys. Rev. B **96**, 245202 (2017).
[38] F. Schweiner, J. Main, and G. Wunner, Phys. Rev. Lett. **118**, 046401 (2017).
[39] G. Dasbach, D. Fröhlich, H. Stolz, R. Klieber, D. Suter, and M. Bayer, Phys. Rev. Lett. **91**, 107401 (2003).
[40] G. Dasbach, D. Fröhlich, H. Stolz, R. Klieber, D. Suter, and M. Bayer, Phys. Status Solidi C **2**, 886 (2005).
[41] G. Dasbach, D. Fröhlich, R. Klieber, D. Suter, M. Bayer, and H. Stolz, Phys. Rev. B **70**, 045206 (2004).
[42] H. Stolz, F. Schöne, and D. Semkat, New J. Phys. **20**, 023019 (2018).
[43] E. Anderson, Z. Bai, C. Bischof, S. Blackford, J. Demmel, J. Dongarra, J. Croz, A. Greenbaum, S. Hammarling, and A. McKenney, *LAPACK Users' Guide,* 3rd ed. (Society for Industrial and Applied Mathematics, Philadelphia, 1999).
[44] F. Schweiner, P. Rommel, J. Main, and G. Wunner, Phys. Rev. B **96**, 035207 (2017).
[45] A. Alvermann and H. Fehske, J. Phys. B **51**, 044001 (2018).
[46] M. Aßmann, J. Thewes, D. Fröhlich, and M. Bayer, Nat. Mater. **15**, 741 (2016).
[47] A. Abragam and B. Bleaney, *Electron Paramagnetic Resonance of Transition Ions*, Oxford Classic Texts in the Physical Sciences (Oxford University Press, Oxford, 2012).
[48] G. Koster, J. Dimmock, R. Wheeler, and H. Statz, *Properties of the Thirty-Two Point Groups*, Massachusetts Institute of Technology Press Research Monograph (M.I.T. Press, Cambridge, MA, 1963).